GEOMATICS, NATURAL HAZARDS AND RISK
2023, VOL. 14, NO. 1, 2221776
https://doi.org/10.1080/19475705.2023.2221776

Research on failure mechanism and support technology of fractured rock mass in an undersea gold mine

Xingdong Zhao[a], Qiankun Zhu[a], Erik Westman[b] and Shanghuan Yang[c]

[a]Geomechanics Research Center, Northeastern University, Shenyang, China; [b]Department of Mining and Minerals Engineering, Virginia Tech, Blacksburg, Virginia, USA; [c]Sanshandao Gold Mine, Shandong Gold Mining (Laizhou) Co., Ltd, Laizhou, China

ABSTRACT

The surrounding rock control has been a difficult problem for fractured rock mass in hard rock mines. This article describes a case study of the failure mechanisms and the support design technology for fractured rock mass drifts in Xinli Gold Mine. Based on field investigation, the geology characteristics, failure types, influencing factors, support types, and their failure types were analyzed. The rock mass classification, rock mass physical and mechanical parameters were obtained by using Q, RMR, and GSI systems. The zoning of surrounding rock, stability analysis and zoning support schemes design were carried out based on rock mass classification results. The pretension is designed by China underground mine experiences and verified by numerical simulation. RS2 was used to compare the plastic zone under pre- and post-support conditions. The plastic zone is significantly reduced after support is installed, which indicates that the designed support schemes can effectively control the failure of surrounding rock. In view of difficulties in the excavation and support of fractured rock mass, the short excavation and short support technology was proposed to ensure the success excavation of the drift in fractured rock mass. The field application shows that the short excavation and support technology are effective.

ARTICLE HISTORY
Received 20 December 2022
Accepted 10 April 2023

KEYWORDS
Fractured rock mass; failure mechanisms; rock mass classification; zoning support; numerical simulation; short excavation and short support technology

1. Introduction

During the process of underground mining and geotechnical engineering construction, fractured rock mass is usually encountered. The fractured rock mass is mainly found in regions with complex geological structure such as faults, altered-zone. The failure of fractured rock mass is affected by many factors, such as the excavation induced stress, ground water, excavation methods, support methods, buried depth, etc. In some special cases, such as water (Zhu et al. 2019; Tang et al. 2022; Liang

CONTACT Qiankun Zhu zhuqiankun1990@126.com Geomechanics Research Center, Northeastern University, Shenyang 110819, China

et al. 2023) and dynamic disturbance (Wang et al. 2022), the engineering mechanical properties of fractured rock mass will deteriorate. If the excavation and surrounding rock control measures are not appropriate, the drifts or underground excavations will suffer from collapse, large deformation (soft rock characteristics), rib spalling, wedge instability, driving face instability, and other failure types, which will affect the development progress, cause serious economic losses, and even lead to casualties.

In recent years, experts and scholars from home and abroad have carried out extensive and in-depth research on the instability characteristics, failure mechanisms, support methods and technology of fractured rock mass under different rock engineering background. The research methods include field investigation, physical experiment, theoretical analysis, numerical simulation, field monitoring and combination method. Toraño et al. (2002) designed two FEM models to study the interaction between fractured rock mass and support. Wang (2005) simulated the interaction of jointed surrounding rock and support of sequential excavation wide-span tunnel using UDEC and self-developed de- and reacting method. Fenhua et al. (2008) quantitatively analyzed the deformation and failure modes of jointed rock mass drifts by using FLAC3D, which was based on regional seismic geology, rock properties, mining conditions and support patterns. Li et al. (2011) established the discrete element numerical model of fractured rock mass drift and analyzed its stress state, plastic zone and deformation features. Senent et al. (2013) developed an advanced rotational failure mechanism to compute the collapse pressure for tunnel faces in fractured rock masses characterized by the Hoek–Brown non-linear failure criterion. Marinos (2014) discussed the standardization of the engineering geological characteristics, the assessment of excavation response and proposed the primary support guidelines for flysch layer qualitatively. Considering the effect of support pressure, bolt presence and partial debonding of bolts, Bouzeran et al. (2017) studied the performance of tunneling at depth under a caving-induced stress path using bonded block model and hybrid-bolt numerical model. Małkowski et al. (2017a, 2017b) studied the roadway stability affected by small throw fault using numerical simulation and in-situ investigation. In order to provide additional insight to rock bolt support mechanisms and forces, Boon (2019) analyzed a wide-span openings in horizontally layered rock using the distinct element method. Du et al. (2020) proposed the support scheme with "short bolt, long anchor cable and two-step grouting shell" to support jointed soft rock drift. To promote liner stability in anisotropic rock mass, Hu et al. (2019) proposed a support system that combines a segmental lining with a highly deformable expanded clay and rock bolts, and performed a series of physical model tests to study the influence factors. Li et al. (2020) studied the deformation failure mechanisms of a deep broken drifts and proposed the "double layer long bolt-mesh-shotcrete and concrete filled steel tube" support scheme.

At present, a variety of support methods and technologies have been put forward for the control of fractured rock mass in underground mining drifts, which solves a large number of supporting problems. However, mining engineering is different from other underground excavation engineering, which has the characteristics of "three-high and one disturbance" (He et al. 2005), namely high in-situ stress, high temperature, high water pressure and mining disturbance. The characteristics of surrounding

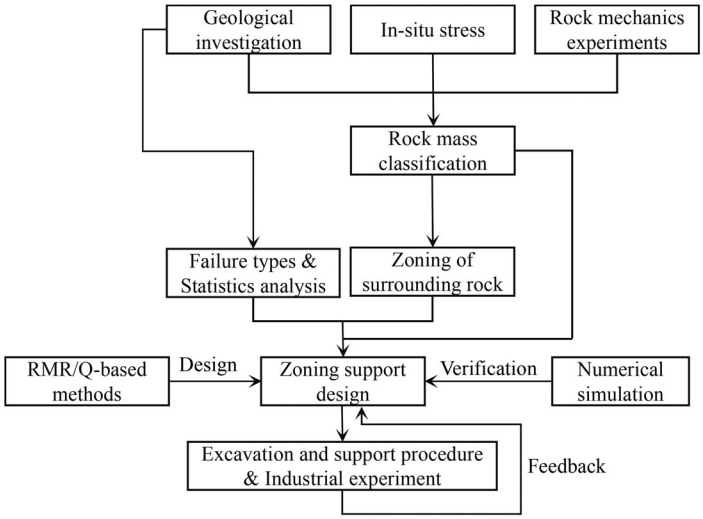

Figure 1. Flowchart of the comprehensive method.

rock, mechanical environment, engineering geological characteristics and mining disturbance of different mines or even different regions of the same mine are significantly different and complex, which leads to the complex engineering problems for the support of fractured rock mass. Therefore, the support of fractured rock mass in underground mines is still a difficult and hot topic in current research. During the drift development in the west region of Xinli Gold Mine, fractured rock mass regions were encountered. The roof of drifts collapsed seriously (up to 13 m), and the roof of driving face collapsed immediately after excavation at some places, resulting in stagnation of mining and driving construction.

In this study, a comprehensive method combined with geological investigation, rock mass classification and numerical simulation was used to design support for drifts in Xinli Gold Mine, a shallow under-sea mine (Figure 1). −200 m to −440 m mining levels were taken as an example to carry out engineering geology survey, rock mechanics experiments, rock mass classification, and zoning the fractured rock mass using rock mass classification results. The failure types, the influencing factors and mechanisms of fractured rock mass are analyzed in detail. On this basis, zoning support schemes were proposed for different regions by using Q and RMR based method, and verified through numerical simulation by using RS2. The pretension is determined by China's experience. The excavation and support procedure for drift with fractured rock mass was designed at the same time. The industrial experiment results verified the excavation and support procedure and also give feedback to support design schemes.

2. Geology background

2.1. The engineering status

Xinli Gold Mine is one of the subordinate mining areas of Sanshandao Gold Mine, located in Laizhou, Shandong Province, China (Figure 2). At present, this mine is the

first under-sea hard rock mine of China, and the orebodies of Xinli Gold Mine are located in the seabed of the Bohai Sea. The average depth of sea water is 10 m, and the orebodies are about 200–2000 m away from the coast. The orebodies occur in −40 m to −700 m under the sea, with a strike of NE 60°, a dip angle of SE 40°–50° and an average thickness of 25 m. The main shaft, service shaft and returned-air shaft are sunk along the coast by using freezing method and curtain-grouting method. After reaching the footwall of the orebody through crosscuts, the development drifts such as the mining level transportation drifts are driven respectively (Figure 3). At present, mining activities are mainly carried out in −200 m level, −360 m level, and −400 m level. The mining method of Xinli Gold Mine is cut-and-fill method. The

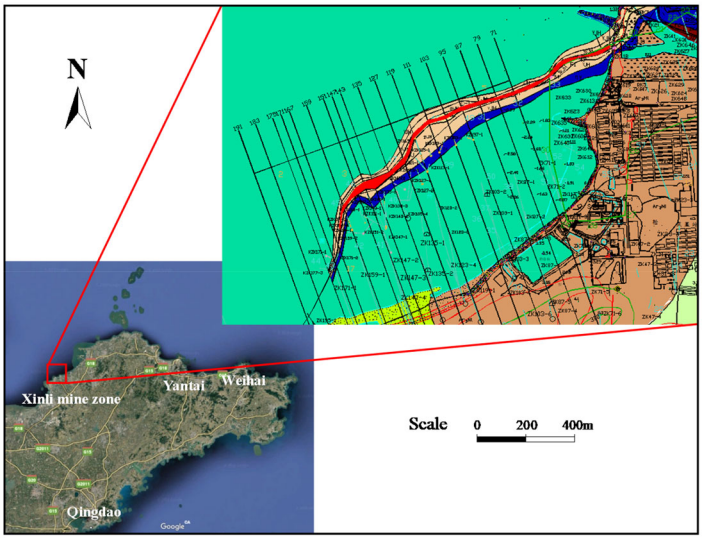

Figure 2. Location and plan view of geological map in Xinli Gold Mine.

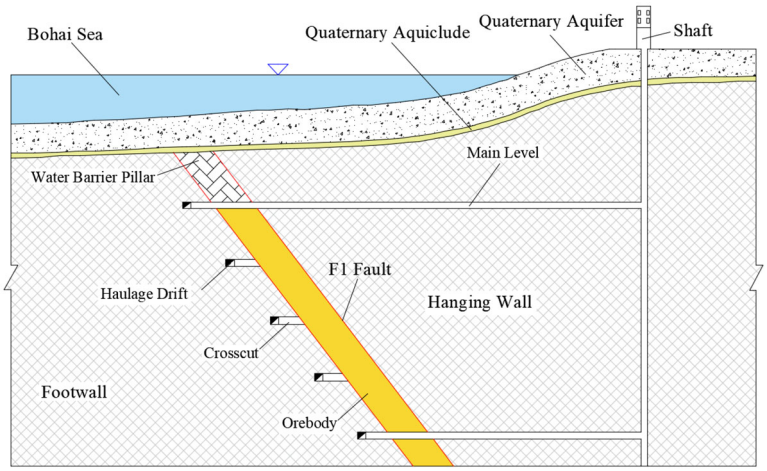

Figure 3. Schematic diagram of under-sea mining of Xinli Gold Mine.

height of the stope is 40 m and the filling material is cemented tailings. The drilling equipment is rock drilling jumbo, and the mucking is self-powered scraper.

2.2. In-situ stress

The stress relief method using improved hollow inclusion cell with complete temperature compensation was employed to measure the in-situ stress in Sanshandao Gold Mine (Miao et al. 2004, 2016). The dip angles of the major principal stress range from −21.3° to 4.0° and close to the horizontal plane. The direction of the major principal stress at 13 measurement points shows good consistency, and all in the direction of WNW-ESE (Figure 4). It is consistent with the direction of the major principal regional tectonic stress. The major principal stress, the intermediate principal stress, and the minor principal stress all increase with depth increasing, and have an approximate linear relationship. The regression equations are shown in Figure 5. In the same depth, although the magnitude and direction of the intermediate principal stress and the minor principal stress have changes, the major principal stress has good consistency and the distribution of in-situ stress field is relatively uniform. At the measurement point at −750 m depth, the difference between the major principal stress and the minor principal stress is 16.12 MPa, which indicates that there is high shear stress at depth, which usually leads to deformation and failure of the surrounding rock.

2.3. Geological structure

Xinli Gold Mine is located in the northwest of Jiaodong Peninsula. The tectonic location is located in Jiaobei uplift area of Jiaobei Terrane in the southern margin of the North China platform. It is adjacent to the Yishu Fault Zone in the west, Jiaolai

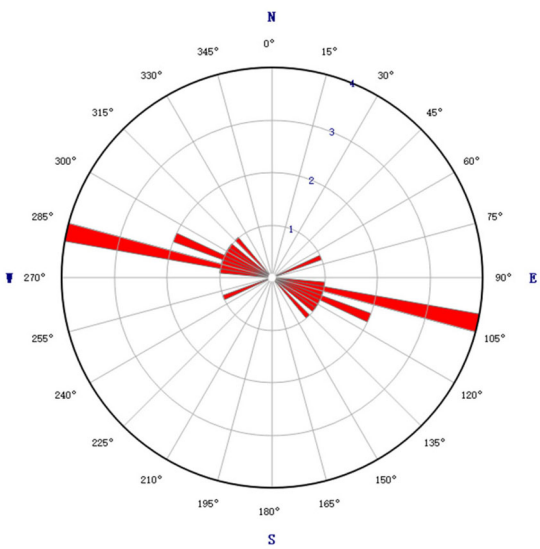

Figure 4. The orientation of the major principal stress (σ_1).

Depression of Jiaobei Terrane in the south, Longkou Fault Basin and Bohai Depression in the north, and Muping-Jimo Tectonic Melange Zone in the East. The ore-forming material (gold) of the deposit mainly comes from metamorphic rock series of greenstone formation of Jiaodong Group. The magmatic hydrothermal solution (rich in gold) of Linglong granite transformed and remelted from Jiaodong Group migrates upward with the addition of atmospheric precipitation to the expansion section of Sanshandao-Cangshang fault, which is precipitated and enriched due to the change of geophysical and chemical conditions. Among the fault structures in the mining area, the largest one is the NE trending Sanshandao-Cangshang fault (F1), the second largest is the NW trending Sanshandao-Sanyuan fault (F3), and the third largest fault is the F2 fault with NNE-ENE trending in the footwall of Sanshandao-Cangshang fault (F1) (Figure 6). F1 fault is a compressional shear fault with developed fault gouge and good water resistance, which is the key to the successful mining of the undersea mine. The internal structure of Sanshandao-Cangshang fault (F1) has horizontal zonation. Along the footwall extension of the F1 fault plane are fault gouge, structural lens, dense joint zone and structural weak zone (Figure 7). On the

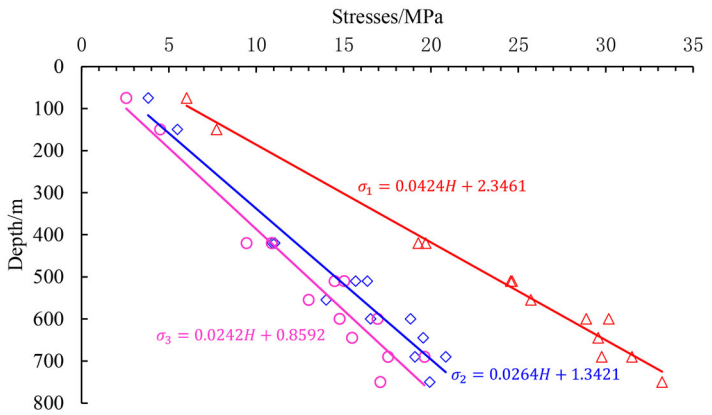

Figure 5. Regression lines of principal stresses with depth.

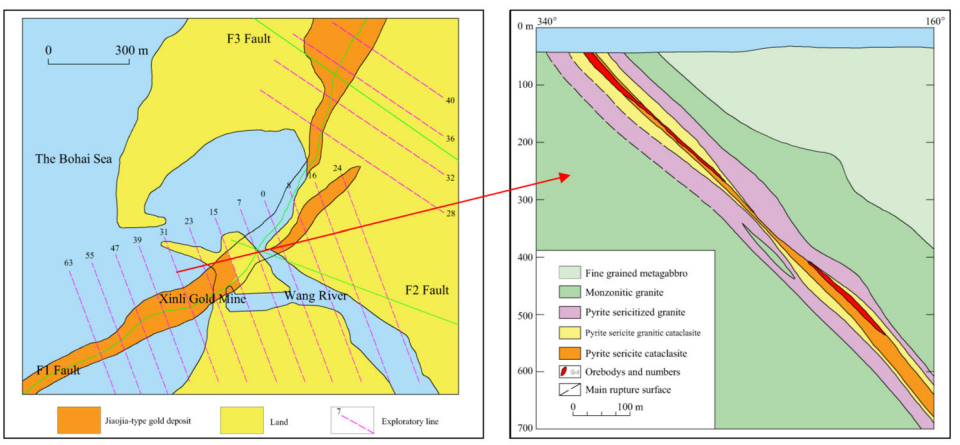

Figure 6. Engineering geological map of Xinli Gold Mine.

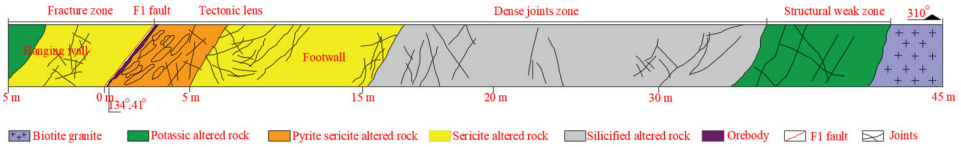

Figure 7. Profile of structural zoning of F1 fault (−375 m level). (Modified from An 2017).

Table 1. Evaluation values for Q and RMR ratings.

Joint parameters	Q rating RMR rating	RQD UCS	Jn RQD	Jr Spacing	Ja Condition	Jw Water	SRF Orientation	Unit weight (gm/cm^3)	UCS (MPa)
Survey locations	−200 m	46.82	15	3.0	4.0	1	2.5	2.718	39.18
	(115–155)	4	8	8	10	10	0		
	−240 m	33.16	15	3.0	4.0	1	2.5	2.718	39.18
	(119–163)	4	8	8	10	10	0		
	−280 m	37.68	12	3.0	4.0	1	2.5	2.722	45.52
	(115–143)	4	8	8	10	10	−10		
	−320 m	35.34	12	3.0	4.0	1	2.5	2.722	45.52
	(115-155)	4	8	8	10	10	−10		
	−360 m	53.85	9	3.0	3.0	1	2.5	2.748	78.15
	(115–123)	7	13	8	20	10	−10		
	−400 m	70.68	9	3.0	3.0	1	2.5	2.748	78.15
	(119–139)	7	13	10	20	10	−10		
	−440 m	63.59	9	3.0	3.0	1	2.5	2.748	78.15
	(115–129)	7	13	10	20	10	−5		

Note: Due to limited field sampling, the physical and mechanical parameters of −200 m and −240 m mining levels are considered to be the same as −212 m rock samples. The physical and mechanical parameters of −280 m and −320 m mining levels are considered to be the same as −307 m rock samples. The physical and mechanical parameters of −360 m, −400 m, and −440 m mining levels are considered to be the same as −373 m rock samples.

hanging wall of the F1 fault plane, there are only structural lens and fracture zone. There was no symmetry between the upper and lower sides. Compared with F2 and F3 faults, F1 fault has large scale and complex tectonic characteristics. The development drifts of Xinli Gold Mine are all arranged in the footwall of orebody. The complicated geological conditions generate some unfavorable factors to the stability of the surrounding rock of the drifts.

2.4. Rock mass classification and zoning of surrounding rock

There are many rock mass classification methods, the most influential and most commonly used rock mass classification methods are Geomechanics Classification or the Rock Mass Rating (RMR) (Bieniawski 1989), Rock Mass Quality (Q) (Barton 2002) and Geological Strength Index (GSI) (Marinos and Hoek 2000). According to the discontinuities investigation results (Table 1) and rock mechanics experiments results (Appendix A), the physical and mechanical parameters required for rock mass quality classification in each mining level are obtained. Three rock mass classification methods are used to classify the quality of fractured rock mass in drift at −200 m to −440 m mining level in southwest part of Xinli Gold Mine (Table 2), and RMR and GSI were assessed independently. The zoning of surrounding rock was according to the rock mass classification results.

Table 2. Evaluation values for RMR, Q and GSI ratings.

Survey locations	RMR_{1989} Rating	RMR_{1989} Description	Q Rating	Q Description	GSI Rating
−200 m (115–155)	40	IV-poor rock	0.94	Very poor	39
−240 m (119–163)	40	IV-poor rock	0.66	Very poor	39
−280 m (115–143)	30	IV-poor rock	0.94	Very poor	44
−320 m (115–155)	30	IV-poor rock	0.88	Very poor	47
−360 m (115–123)	48	III-fair rock	2.39	Poor	56
−400 m (119–139)	50	III-fair rock	3.14	Poor	56
−440 m (115–129)	55	III-fair rock	2.83	Poor	63

Table 3. Material constants, tensile strength, cohesion force, and internal angle of rock mass.

Survey locations	mb	s	a	σ_{tmass} (MPa)	c' (MPa)	φ' (°)
−200 m (115–155)	2.2351	0.0005	0.5122	0.0094	0.84	43.77
−240 m (119–163)	2.2351	0.0005	0.5122	0.0094	0.94	42.41
−280 m (115–143)	2.7576	0.0010	0.5087	0.0164	1.19	44.21
−320 m (115–155)	3.1280	0.0014	0.5070	0.0210	1.36	44.26
−360 m (115–123)	4.5656	0.0044	0.5038	0.0749	2.08	50.48
−400 m (119–139)	4.5656	0.0044	0.5038	0.0749	2.22	49.73
−440 m (115–129)	6.1268	0.0104	0.5023	0.1324	2.75	50.93

Table 4. Estimated elastic modulus E_{mass} of rock mass.

Survey locations	Equation no. (4)	(5)	(6)	(7)	(8)	(9)	(10)	(11)	(12)	(13)	(14)	E Average (GPa)
−200 m (115–155)	5.62	NA	NA	3.28	11.69	4.94	6.40	7.17	2.82	7.13	3.26	5.81
−240 m (119–163)	5.62	NA	NA	3.28	11.69	5.22	6.40	6.37	2.82	7.13	3.26	5.75
−280 m (115–143)	3.16	NA	NA	2.27	7.99	2.98	2.70	7.54	4.06	9.50	5.20	5.05
−320 m (115–155)	3.16	NA	NA	2.27	7.99	3.10	2.70	7.37	4.83	10.22	6.35	5.33
−360 m (115–123)	8.91	NA	9.46	6.21	21.04	9.57	11.06	12.31	10.61	15.04	12.95	11.72
−400 m (119–139)	NA	NA	12.42	6.76	22.45	11.15	12.50	13.49	10.61	15.04	12.95	13.04
−440 m (115–129)	NA	10.00	11.29	8.31	25.96	15.74	16.64	13.03	15.88	17.94	18.68	15.35

2.5. Estimation of rock mass properties

The Hoek–Brown parameters (m_b, s, a), tensile strength of rock mass (σ_{tmass}) and equivalent Mohr–Coulomb strength parameters (c', φ') were obtained by using Rocdata (RocData), see Table 3, and GSI values are shown in Table 2, where m_b, s, and a are the rock mass material constants. The surrounding rock type is pyrite sericite cataclastic granite, and its m_i value is 29. The variable "D" is the rock mass disturbance factor. For the study area, the smooth blasting effect is poor, so the value is considered to 0.3. Rock mass deformation modulus (E_{mass}) were calculated by means of different empirical equations (Appendix B) by using rock mass classification result (Table 4). These are the input data for the numerical simulation.

3. Failure types, influence factors, and mechanisms of fractured rock mass

3.1. Failure types

In order to explore the spatial distribution of the fractured rock mass and the failure characteristics of the surrounding rock, a detailed engineering geological

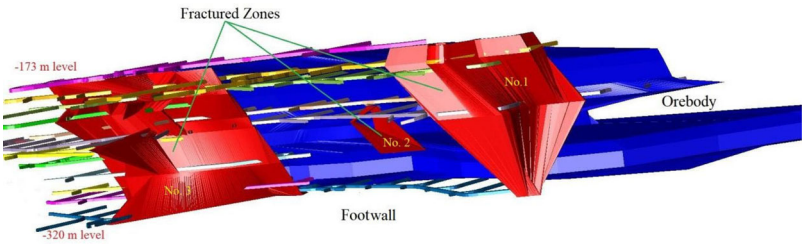

Figure 8. Fractured zones in the study area.

Figure 9. Surrounding rock failure types.

investigation was carried out on the drifts and crosscuts from −173 m level to −440 m level at the southwest zone of Xinli Gold Mine. The fractured zones above −320 m level are marked in the 3D model of the mine (Figure 8). There are three fractured zones in this region, among which No. 3 is the largest one. There are fewer development drifts below −320 m level, and the fractured rock mass is not fully exposed, so the range of the fractured zones were not delineated. The reasons for the formation of fractured zone are as follows: the rock mass suffered multiple tectonic movements, resulting in extremely developed joints, and low strength of surrounding rock caused by long-term alteration.

According to the field investigation, the failure characteristics of drifts can be divided into four types, including roof collapse, wedge instability, squeezing deformation and rib spalling (Figure 9). The statistics of each failure type is shown in Figure 10.

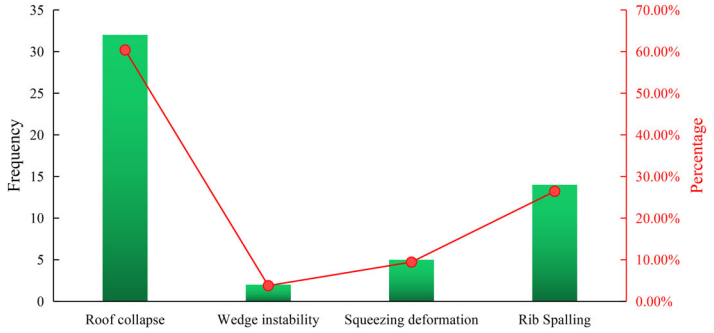

Figure 10. Statistics of different failure types.

The roof collapse mostly occurs at the dense joints zone, and the rock mass looks like "sugar cubes." One of the drift roof falls resulted in a collapse of the roof up to 13 m above the entry. Rib spalling mainly occurs in the relatively intact rock mass of the drift, at T-shaped or Y-shaped intersections. Some zones apparently present rock mass sliding. Under the tectonic stress, gravity and induced stress conditions, the drift undergoes squeezing deformation, which is manifested as asymmetric deformation on both sides or roof squeezing deformation. There are fewer wedge instability cases, which is caused by the potential falling rocks in the roof being removed regularly.

3.2. Influence factors

3.2.1. Excavation-induced stress

Considering that the mining depth is shallow, the in-situ stress is not too high, and most part of the ore body has not been mined, so the source of high stress is mainly from excavation-induced stress. The stress concentration in the surrounding rock is caused by excavation activities leading to the high stress failures. For example, rib spalling and squeezing deformation in large-scale excavation and drift intersections.

3.2.2. Rock mass structure

Under the influence of complex tectonic movement, the joints are very developed, and some of the rock mass appears like "sugar cubes." Some rock mass is loose, the loading capacity is reduced, and the roof falls continuously, and some locations cave up to the upper level drift. The support structure bears the loose rock mass falling directly, which causes bending deformation of the top and/or legs of U-shaped steel support.

3.2.3. Blasting vibration

The mining method of Xinli Gold Mine is cut-and-fill method. The amount of mine development work is large and the underground excavation blasting activities are frequent. Blasting vibration can accelerate the slip of rock mass along weak interface and the collapse process of fractured rock mass in the roof. And the blasting operation also will cause damage to the surrounding rock.

3.2.4. Underground water

Although Xinli Gold Mine is located under the sea, the water inflow in the development drifts is less, and the permeability and water content of the surrounding rock are poor, so the underground water has little effect on the stability of most drifts. However, if there is a fractured rock mass zone, the water in the drift will slowly penetrate to the next mining level along fractures. With the action of water and alteration or fault gouge, it is easy to cause the rock block sliding or falling off along the fracture planes. Furthermore, the underground water in the mining area is mainly Paleosea water, which is Cl–Na type water, and it has the characteristics of highly mineralized saline water. Most of the water samples show weakly acidic characteristics. The chemical damage of underground water to rock mass will affect the stability of surrounding rock at some places, this should be studied in the future.

3.3. Failure mechanisms

3.3.1. Roof collapse

Due to the extremely developed fractures in surrounding rock, there are multiple groups of cross fractures. Under the action of gravity, and affected by blasting vibration or/and fissure water, roof collapse will occur to varying scales until the stable pressure arch is formed (Figure 11).

3.3.2. Wedge instability

If there are three structural planes or more groups of structural planes in the roof of drifts, one or more wedges can be formed. If the wedge cannot be constrained by the surrounding rock, it will fall into the drift (Figure 12). The potential motion of wedges can be analyzed by stereographic projection method.

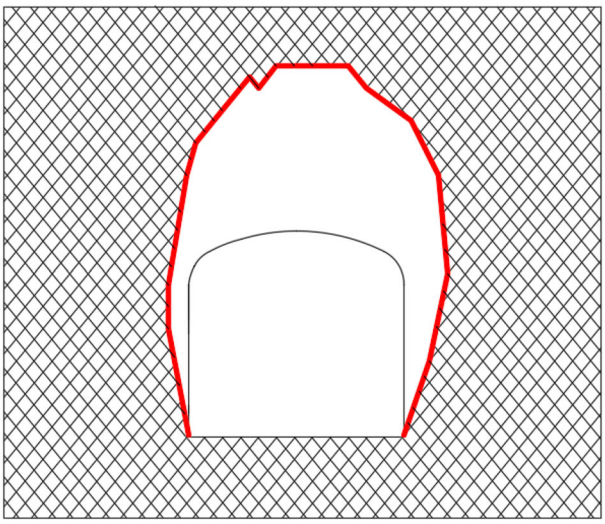

Figure 11. Schematic of roof collapse.

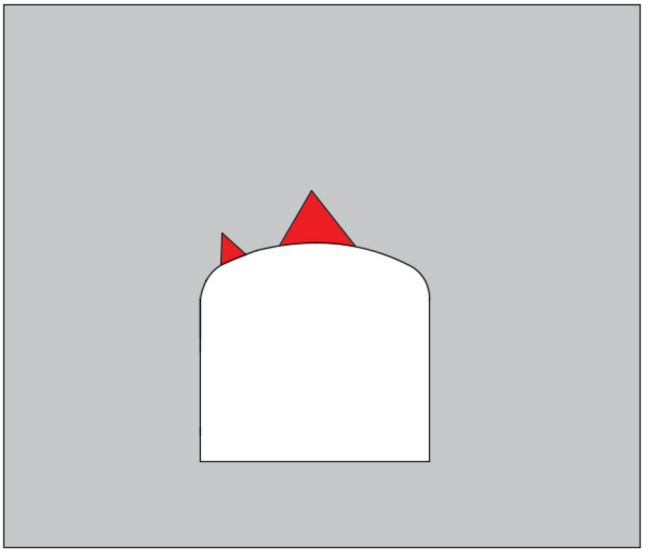

Figure 12. Schematic of wedge instability.

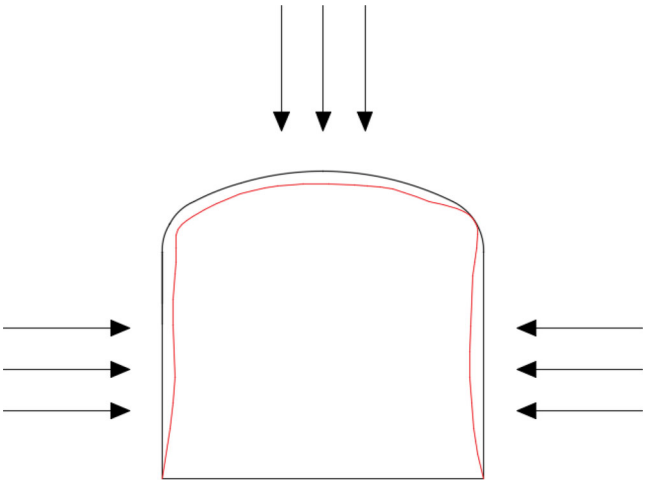

Figure 13. Schematic of squeezing.

3.3.3. Squeezing

When the weak surrounding rock drift is subjected to large top and/or lateral stress, such as horizontal tectonic stress, mining-induced vertical stress and gravity of loose rock mass in the roof, the top of the basket-handle arch drift will be flattened, the two sidewalls will be extruded (Figure 13).

3.3.4. Rib spalling

In the intact brittle surrounding rock drifts, especially the drift intersections or large-span drifts, after the drift excavation, high excavation-induced stress will be formed around the drift, especially the vertical stress acting on the sidewalls will increase

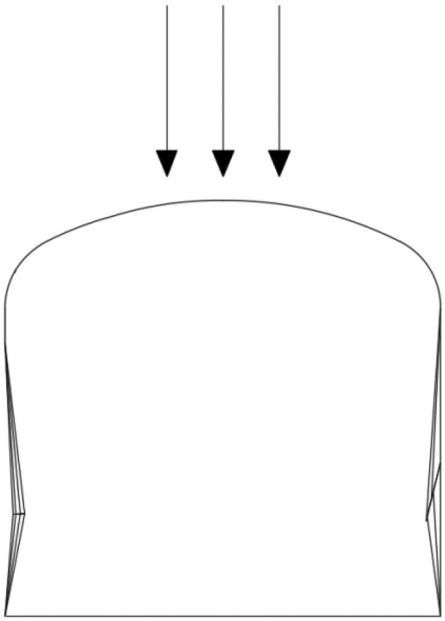

Figure 14. Schematic of rib spalling.

significantly, and the horizontal deformation of the sidewalls will cause horizontal tensile fracture in the surrounding rock, as shown in Figure 14. If the longitudinal direction fractures are developed in the sidewalls, it will aggravate the occurrence of such damage.

4. Support design of fractured rock mass

4.1. Failure types of the support

There are six kinds of support types of fractured rock mass in southwest zone of Xinli Gold Mine: shotcrete, I-beam steel shed, U-shaped steel, masonry-lining, slit wedge tubing bolt and combination support. All the above support types are passive support, and the supporting force is applied to the surrounding rock directly after deformation of surrounding rock, and then the support itself to resist the further deformation and failure of surrounding rock. The disadvantage of passive support is that it is difficult to resist further deformation and failure of surrounding rock after deformation, especially in high-stress, fractured or weak conditions (Hou 2013). The failure types of support in this mine are U-shaped steel arch frame bending in the roof, masonry-lining cracking, shotcrete layer spalling, I-beam steel bending/buckling and corrosion Figure 15. To a certain extent, old support types can meet the support needs, but the drifts excavation speed is slow, cost is high, and quality cannot be fully guaranteed. Furthermore, the Paleo-ocean water is extremely corrosive, which will intensify the corrosion rate and degree of the metal components of support, and seriously affect the stability of the supporting structure. With the increase of mining depth and the impact of complex geological conditions, the stability of drifts

Figure 15. Failure types of support.

surrounding rock can no longer be completely and effectively controlled. Therefore, a new support scheme is required.

4.2. Zoning support design based on RMR and Q classification systems

Different empirical methods are used to evaluate rock mass stability and to design an appropriate support system, including a support design method based on RMR and Q rock mass classification. The parameters of bolt, shotcrete, mesh, and U-shaped steel support can be determined by empirical methods. Bieniawski(1989) proposed the support guidelines for engineering rock mass based on RMR_{89} system. Bieniawski's support guidelines usage is limited to tunnels with a horseshoe shape, 10 m width, vertical stress

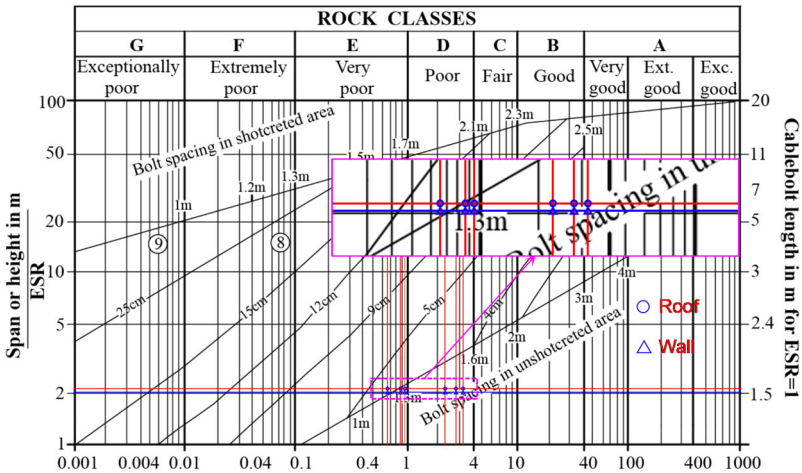

Figure 16. Support chart of Q system.

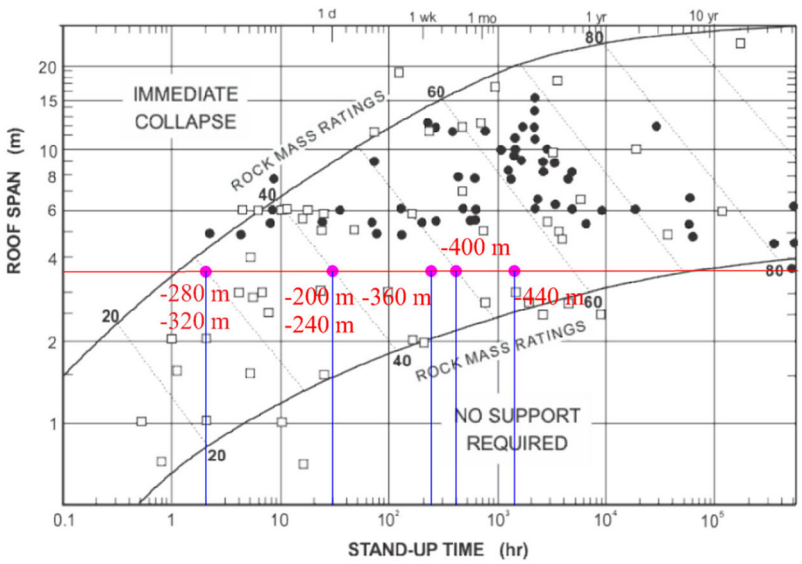

Figure 17. Stand-up time of drifts.

below 25 MPa and drill and blast method for excavation conditions. However, Lowson and Bieniawski (2013) created new design charts for rock bolt, shotcrete, and steel ribs. In the new design charts, the selection of rock support works as a function of both tunnel size and rock mass quality, it can also help to decide the tunnel shape and secondary liners. The support design based on Q system is found by using the support chart (Grimstad 1993). The equivalent dimension (D_e) of excavation is obtained by:

$$D_e = \frac{\text{Excavation span, diameter or height (m)}}{\text{Excavation support ratio (ESR)}}, \tag{1}$$

where ESR values range from 0.5 to 5. The detailed values were given in a table by

Barton et al. (1974). In this study we set the ESR to 1.6. As the span and height of the drifts are 3.6 m and 3.3 m respectively, the equivalent dimensions (D_e) are 2.25 m for roof and 2.06 m for walls. The newest design chart was updated by Grimstad (1993). The new chart considers the usage of steel fiber reinforced shotcrete. However, when Q and equivalent dimension values are plotted in Figure 16, we can find that no drift support is required, which is obviously unreasonable. According to the stand-up time chart of the rock mass (Figure 17) and the in-situ survey, the stand-up time of the rock mass within the study area is from 2 h to about 2 months, and most of them shorter than 3 weeks.

In this research, the shotcrete thickness and rib support selection were based on RMR_{89} support guidelines. The following equations were used to design bolt spacing, bolt length:

$$\text{Rock bolt spacing } S_b = \begin{cases} 0.5 + 2.5\dfrac{RMR - 20}{65}, & 20 < RMR \leq 85 \\ 0.25 + \dfrac{(RMR - 10)^{1.5}}{140}, & 10 < RMR \leq 20 \\ 0.25, & RMR \leq 10 \end{cases}, \tag{2}$$

$$\text{Rock bolt length Span} = \frac{(L_b + 2.5)^{\frac{RMR+25}{52}}}{3.6}, \tag{3}$$

or

Table 5. Support categories for selected sites.

	RMR89		Q		
Survey locations	Rating	Support requirements	Rating	Support requirements	Adopted support design
−200 m (115–155)	40		0.94	Unsupported	Rock bolts 2.5 m long, spaced 1.2 m in crown and walls with wire mesh; shotcrete 100 mm in crown, sidewalls and floor
−240 m (119–163)	40	Systematic bolts 4–5 m long, spaced 1–1.5 m in crown and walls with wire mesh; 100–150 mm in crown and 100 mm in sides; Light ribs spaced 1.5 m where required.	0.66	Systematic bolting and unreinforced shotcrete, 4–10 cm	
−280 m (115–143)	30		0.94	Unsupported	Rock bolts 2.5 m long, spaced 0.8 m in crown and walls with wire mesh; shotcrete 100 mm in crown, sidewalls and floor
−320 m (115–155)	30		0.88	Unsupported	
−360 m (115–123)	48		2.39	Unsupported	Rock bolts 2.5 m long, spaced 1.5 m in crown and walls with wire mesh; shotcrete 100 mm in crown, sidewalls and floor
−400 m (119–139)	50	Systematic bolts 4 m long, spaced 1.5–2 m in crown and walls with wire mesh in crown; 50–100 mm in crown, and 30 mm in sides.	3.14	Unsupported	
−440 m (115–129)	55		2.83	Unsupported	

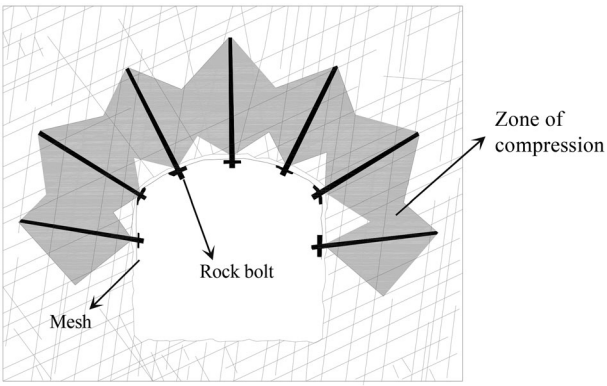

Figure 18. Artificial pressure arch.

$$L_b = 2 + \frac{0.15B \text{ or } H}{ESR}, \tag{4}$$

The rock bolt length obtained by Equation (3) is too long to be installed in the drift, and the calculated values are discarded, so Equations (4) was used to calculate the rock bolt length (Barton et al. 1974). The estimated support categories based on Q-system for each site have been shown in Table 5. The estimated support is correctly design only if no mining disturbance occurs.

4.3. Pretension design

The function of rock bolting is to construct of an artificial pressure arch, also called self-support arch (Figure 18). This arch is a zone of compressive stress, where rock blocks are interlocking with the help of rock bolts. When the artificial pressure arch is formed, the rock bolts and the rock blocks within its reinforcement range will form a stable load-bearing structure, resisting the self-weight of the upper rock mass and excavation or mining induced stress, and avoiding roof fall and collapse of the drifts with fractured rock mass. The formation of artificial pressure arch is affected by many factors, such as rock bolt support patterns and parameters, surrounding rock structure and properties. Under a given rock bolt layout scheme, pretension is a key parameter for forming an artificial pressure arch. Pretension is the pre-loaded axial tensile force on rock bolts. Pretension also can improve the active load-carrying capacity of the rock bolts. Mesh and shotcrete can help to retain rock blocks in zones without stress between rock bolts. The formation of artificial pressure arch under the same pretension is related to the density of rock bolts, and the denser the rock bolts, the easier it is to form artificial pressure arch. Therefore, the low-density bolt support design scheme is selected for pretension design.

The principle of rock bolt pretension design is to control the surrounding rock to avoid obvious layer separation, sliding or tensile stress zone. Mines in China generally use 30–50% of the yield load of the rock bolt as the pretension (Kang and Wang 2007). The yield load of the BHRB335 rock bolt with a diameter of 22 mm is 125 kN, and the breaking load is 185 kN. Combined with the site equipment and drift

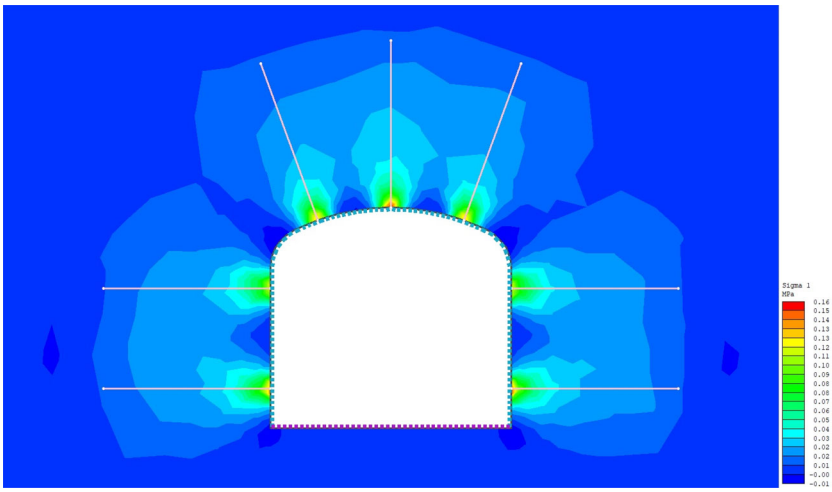

Figure 19. Pretension stress field.

conditions, the design pretension value is 60 kN (about 50% of yield load). In order to verify the rationality of the designed pretension, the numerical simulation is used to analyze the pretension stress field of the low-density rock bolt support. The physical and mechanical parameters of the rock mass at the −400 m level are applied. It can be seen from Figure 19, under the given rock bolt layout and designed pretension, the pretension can make the rock bolts in the surrounding rock within its reinforcement range building a continuous pretension stress field. The continuous pretension stress field helps to make the surrounding rock within the reinforcement range a stable load-bearing structure, that is, to form an artificial pressure arch, improve the bearing capacity of the surrounding rock, and prevent the instability and failure of the surrounding rock, especially in the roof. Research by Kang et al. (2014), Li et al. (2020) shows that the pretension stress field formed by rock bolts in the surrounding rock is 0–0.4 MPa, and the stress field in Figure 19 is 0–0.16 MPa, this shows that the rationality and effectiveness of the designed pretension.

4.4. Numerical simulation of the support schemes

In order to verify the results of the support schemes, RS2 (Rocscience 2022a, 2022b) was used to calculate the thickness of the plastic zones around drifts due to the excavation and after installation of rock support. This program is based on the finite element analysis by using the Mohr-Coulomb failure criterion. The shape of the drifts is basket-handle arch (with height of 3.3 m and width of 3.6 m), the expansion factor of the external boundary is 3.0. The external boundaries are all fixed. Graded mesh type with three noded triangles element type was chosen for mesh discretization. The constant field stress type was calculated by Equations in Figure 5. Considering the complex geological structure in this mine, it is assumed that the drifts are in the most unfavorable situation, that is, the major principal stress is perpendicular to the strike of drift, the intermediate principal stress is parallel to the strike of drift, and the minor principal stress is in vertical direction. The input parameters such as

shown in Tables 4 and 5. The Poisson's ratio directly used the values from unconfined compression tests. The plastic zone and the reduced plastic zone analysis was done for different levels for pre- and post-support conditions. The analysis indicates that without support, the plastic zones in the drift roof, floor and sidewalls at −200 m to −320 m level are larger than that of −360 m to −440 m level drifts. After the installation of support, the plastic zones of drifts at different levels has reduced, especially in the drift roof, while the plastic zones in floor showed a limited decrease in the size of the plastic zone. It shows that the designed support schemes can effectively control the failure of surrounding rock (Figure 20).

Taking the numerical simulation results of unsupported drift at the −400 m level as an example, in terms of failure types of surrounding rock, the failure type of the shallow surrounding rock of the drift is mainly tensile failure, while the failure type of the deep surrounding rock is mainly shear failure (Figure 21). The excavation and unloading of the surrounding rock of the drift will lead to tensile failure in the

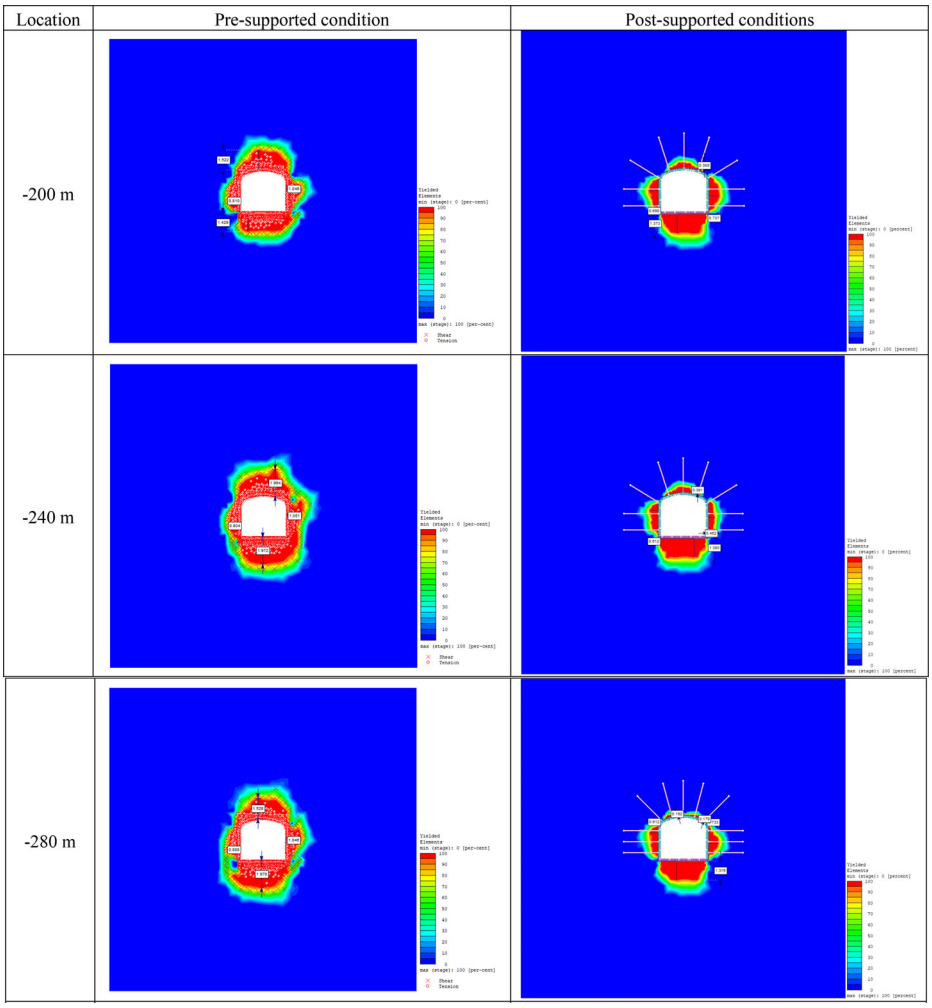

Figure 20. Plastic zone distribution under pre-support and post-support conditions.

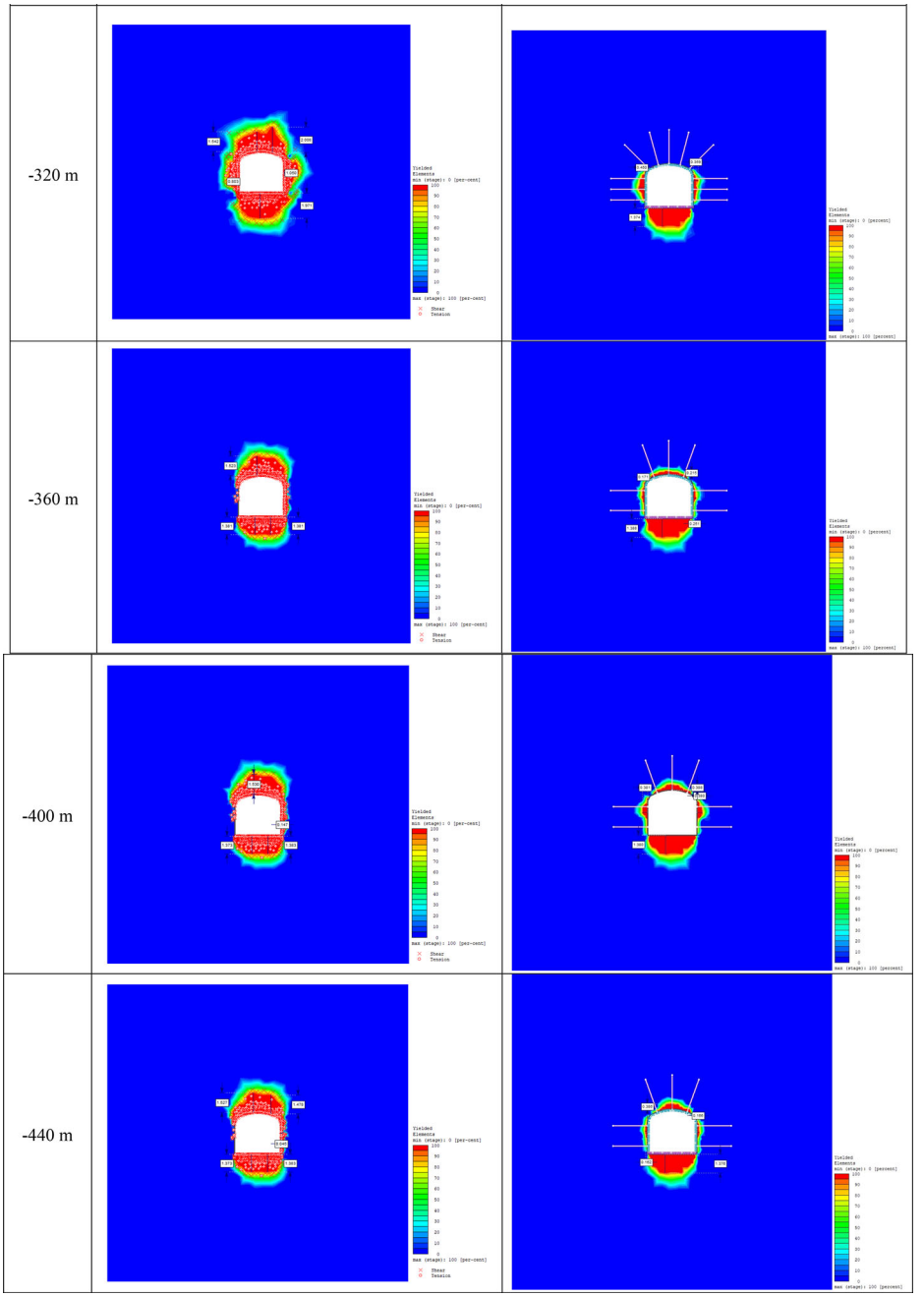

Figure 20. Continued

shallow surrounding rock, the major principal stress of the shallow surrounding rock will decrease, and the high stress zone will transfer to the deep surrounding rock. The larger deviatoric stress will lead to shear failure of the deep surrounding rock. It can also be seen from Figure 21 that there is a critical maximum shear strain for the surrounding rock failure of the drift. When this value is exceeded, the surrounding

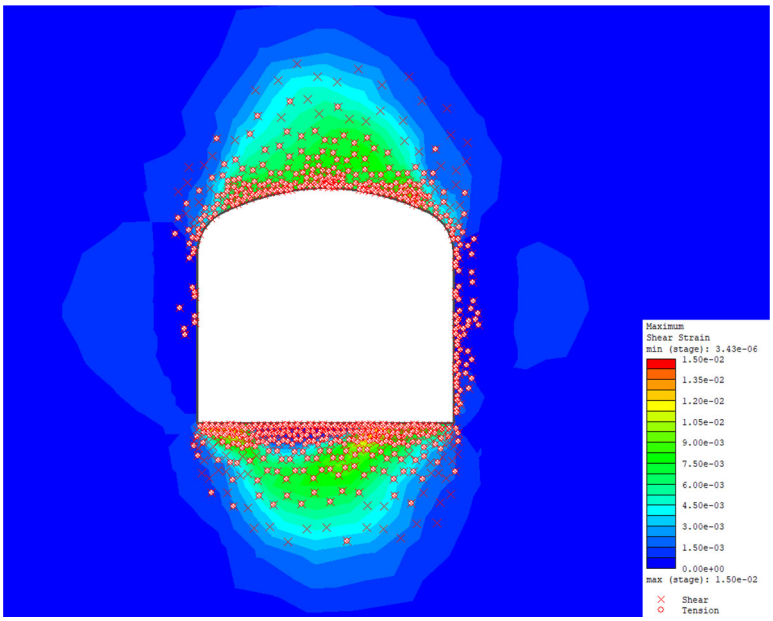

Figure 21. Failure types and distribution of maximum shear strain.

rock will undergo shear failure, which is the outermost boundary of the failure zone. In the example given, the critical maximum shear strain value is about 1.5‰.

5. Excavation and support procedure of fractured rock mass and engineering application

In the fractured rock mass, the stability of the surrounding rock of the drift is very poor, and it can hardly maintain stability after excavation or the stand-up time is very short, which will cause severe roof fall accidents. In view of this kind of rock mass, the short excavation and short support technology is proposed (Figure 22). The specific procedure is as follows:

1. When the fractured zone is exposed, bolt-mesh-shotcrete support should be carried out at 3 ~ 5 m in front of the fractured zone to form an integral structure of rock mass and support, and improve the stability of surrounding rock around the junction place.
2. After the support in (1) is completed, the drift should be driven forward for 2 m (i.e. the blast hole depth). Smooth blasting technology should be used in drift excavation with fractured surrounding rock. More blast holes should be drilled and less charge should be used to minimize the disturbance of blasting vibration on surrounding rock of drifts.
3. After blasting, the rock is mucked and a 5-cm thick shotcrete layer is sprayed on the new exposed rock mass. If the stand-up time of the surrounding rock after blasting is too short to complete the rock mucking, then temporary support (such as steel set and wood support) should be installed first, and then removed the blasted rock fragments.

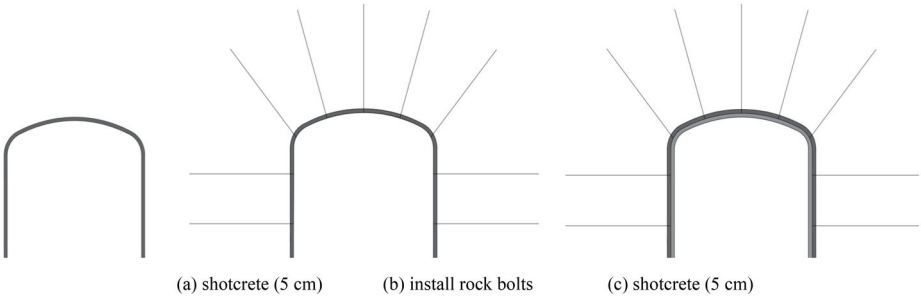

Figure 22. Support procedure of the drift.

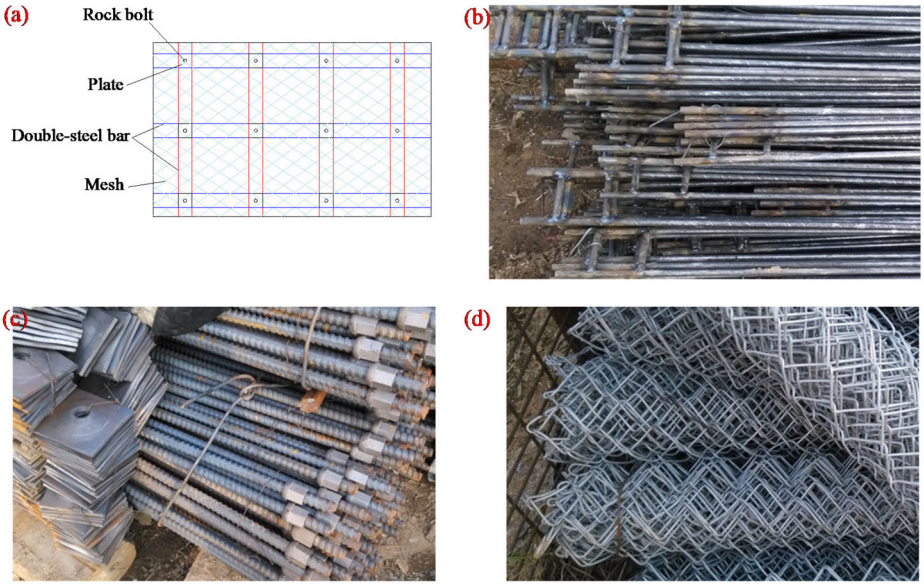

Figure 23. Layout of rock bolts, mesh, and double-steel bars.

4. Bolt-mesh is installed in the surrounding rock of the 2-m long drifts and double-steel bars are used accompanied with rock bolt and mesh (Figure 23). The overlapping length of mesh shall not be less than 20 cm, which should be bound with iron wire with diameter of 3.5 mm. Then sprayed with another layer of shotcrete with 5 cm thickness. The purpose is to make the rock bolt, mesh and shotcrete layer form the strengthening beam and improve the support capacity of the support structure.
5. The next round of excavation is completed by driving 2 m forward again. Repeat Steps (2)–(4) to form the next working cycle of bolt-mesh-shotcrete combined support.

The supported drift is shown in Figure 24, this photo was taken nine months after the support was installed. It can be seen from the photo that the proposed support scheme maintained the stability of fractured rock mass drift. Compared with the

Figure 24. Filed implementation of the support (No. 141 crosscut at −212 m).

previous support, the bolt-mesh-shotcrete support has the following advantages: (1) the installation of the bolt-mesh-shotcrete support is simple and the cost is low, which is conducive to the mine cost reduction and efficiency increase; (2) the installation time of the bolt-mesh-shotcrete support is much shorter than that of the previous support, which can ensure the rapid and safe drift excavation; (3) the previous support belongs to passive support, which can't prevent the further caving of drift roof; while the bolt-mesh-shotcrete support can form pressure bearing arch and give full play to the self-stability of surrounding rock; (4) by adjusting the spacing of bolt and combining with temporary support, it can be applied to different fractured rock mass conditions and can effectively control the deformation and failure of fractured rock mass.

6. Conclusion

Stability control of the fractured rock mass in Xinli Gold Mine restricted the rate of development and mining, especially for its special engineering background. The drifts were excavated in fractured rock mass in the shallow under-sea mine. In this article, a comprehensive method based on field observation, rock mass classification and numerical simulation was proposed to select rock support schemes and determine pretension. The excavation and support procedure of fractured rock mass is given at the same time. The main conclusions are as follows:

1. According to the field investigation, the engineering geological characteristics, drift failure types, influencing factors, support types and failure modes were analyzed in detail. The failure types of drift included roof collapse, wedge instability, squeezing deformation and rib spalling. The main influencing factors are excavation-induced stress, rock mass structure, blasting vibration and underground water.

2. The existing support forms are shotcrete, I-beam steel shed, U-shaped steel, masonry-lining, slit wedge tubing bolt and combination support, and the support effect is not acceptable. The failure types include U-shaped steel arch frame bending in the roof, masonry-lining cracking, shotcrete layer spalling and I-beam steel bending, corrosion.
3. The engineering geological survey and rock mechanics tests were carried out, and the rock mass classification and mechanical parameters estimation were carried out. According to the empirical method, the support schemes for fractured rock mass in different regions are given. The pretension value of the designed support is 60kN, and verified the rationality and effectiveness of forming artificial pressure arch using numerical simulation.
4. The RS2 numerical simulation software was used to analyze the distribution characteristics of the plastic zone in the surrounding rock under the pre-support and post-support conditions. The plastic zone of the surrounding rock (especially in the roof) is significantly reduced after support installed, which indicates that the designed support schemes can effectively control the failure of surrounding rock. In view of the excavation and support of fractured rock mass, the short excavation and short support technology is proposed to ensure the success construction of the drift in fractured rock mass. The field application shows that the short excavation and support technology are effective.

Acknowledgments

We would like to thank the mining engineers and workers for their help in field survey and industrial test.

Disclosure statement

No potential conflict of interest was reported by the authors.

Funding

This research was funded by the Key Program of National Natural Science Foundation of China (52130403), Liaoning Provincial Central Leading Local Science and Technology Development Special Project (2023JH6/100100050) and the China Scholarship Council (201906080107).

References

An P. 2017. Ore-controlling model of permeability structures in fault zone, Sanshandao gold deposit, Shandong Province, China. Beijing: China University of Geosciences (Beijing).

Barton N. 2002. Some new Q-value correlations to assist in site characterisation and tunnel design. Int J Rock Mech Min Sci. 39(2):185–216.

Barton N, Lien R, Lunde J. 1974. Engineering classification of rock masses for the design of tunnel support. Rock Mech. 6(4):189–236.

Barton N, Løset F, Lien R, Lunde J. 1981. Application of Q-system in design decisions concerning dimensions and appropriate support for underground installations. In Subsurface space. Stockholm, Sweden: Elsevier; p. 553–561.

Bieniawski ZT. 1978. Determining rock mass deformability: experience from case histories. Int J Rock Mech Min Sci Geomech Abstr. 15(5):237–247.
Bieniawski ZT. 1989. Engineering rock mass classifications: a complete manual for engineers and geologists in mining, civil, and petroleum engineering. New York: John Wiley & Sons.
Boon C. 2019. Study of reinforcement support mechanisms for wide-span horse-shoe-shaped openings in horizontally layered jointed rock using the distinct element method. Rock Mech Rock Eng. 52(4):1179–1191.
Bouzeran L, Furtney J, Pierce M, Hazzard J, Lemos J. 2017. Simulation of ground support performance in highly fractured and bulked rock masses with advanced 3DEC bolt model. In: Deep Mining 2017: Proceedings of the Eighth International Conference on Deep and High Stress Mining. Johannesburg: Australian Centre for Geomechanics; p. 667–680.
Du S, Li D, Yu W, Zhang J, Liu F. 2020. Stability analysis and support control for a jointed soft rock roadway considering different lateral stresses. Geotech Geol Eng. 38(1):237–253.
Fenhua R, Xingping L, Meifeng C, Zhaohai L, Lei Z, Xin C, Libo L. 2008. Quantitative prediction and evaluation on the regularity of asymmetric damage and distortion upon broken rock mass roadways. Chin J Eng. 30(3):221–226.
Grimstad E. 1993. Updating the Q-system for NMT. In: Proceedings of the International Symposium on Sprayed Concrete-Modern Use of Wet Mix Sprayed Concrete for Underground Support, Norwegian Concrete Association, 1993. Fagemes, Oslo, Norway.
He MC, Xie HP, Peng SP, Jiang YD. 2005. Study on rock mechanics in deep mining engineering. Chin J Rock Mech Eng. 24(16):2803–2813.
Hoek E, Diederichs MS. 2006. Empirical estimation of rock mass modulus. Int J Rock Mech Min Sci. 43(2):203–215.
Hou C. 2013. Ground control of roadways. Xuzhou: China University of Mining and Technology Press.
Hu X, Fang Y, Walton G, He C. 2019. Analysis of the behaviour of a novel support system in an anisotropically jointed rock mass. Tunn. Undergr. Space Technol. 83:113–134.
Kang H, Jiang P, Cai J. 2014. Test and analysis on stress fields caused by rock bolting. Journal of China Coal Society. 39(8):1521–1528.
Kang H, Wang J. 2007. Rock bolting theory and complete technology for coal roadways. Beijing: China Coal Industry Publishing House.
Li G, Ma F, Guo J, Zhao H, Liu G. 2020. Study on deformation failure mechanism and support technology of deep soft rock roadway. Eng Geol. 264(March):105262.
Li J, Kang H, Gao F, Lou J. 2020. Analysis of bolt support stress field and bolt support effect under in-situ stress field. J China Coal Soc. 45(s1):99–109.
Li S, Wang L, Lu Y. 2011. Numeriacl simulation for deformation failure characters in roadway with broken rock mass. J. Min. Saf. Eng. 28(1):39–44.
Liang X, Tang SB, Tang CA, Hu LH, Chen F. 2023. Influence of water on the mechanical properties and failure behaviors of sandstone under triaxial compression. Rock Mech Rock Eng. 56(2):1131–1162.
Lowson AR, Bieniawski ZT. 2013. Critical assessment of rmr-based tunnel design practices: a practical engineer's approach. Proceedings – Rapid Excavation and Tunneling Conference (June):180–198.
Małkowski P, Ostrowski L, Bachanek P. 2017a. Modelling the small throw fault effect on the stability of a mining roadway and its verification by in situ investigation. Energies 10(12): 2082.
Małkowski P, Ostrowski L, Bachanek P. 2017b. The impact of the low throw fault on the stability of roadways in a hard coal mine. Stud. Geotech. Mech. 39(1):63–72.
Marinos P, Hoek E. 2000. GSI: a geologically friendly tool for rock mass strength estimation. In: ISRM International Symposium. Melbourne: International Society for Rock Mechanics and Rock Engineering.
Marinos V. 2014. Tunnel behaviour and support associated with the weak rock masses of flysch. J Rock Mech Geotech Eng. 6(3):227–239.

Miao S, Wan L, Lai X, Wang S. 2004. Relation analysis between in-situ stress field and geological tectonism in Sanshandao gold mine. Chin J Rock Mech Eng. 23(23):3996–3999.
Miao SJ, Cai MF, Guo QF, Huang ZJ. 2016. Rock burst prediction based on in-situ stress and energy accumulation theory. Int J Rock Mech Min Sci. 83:86–94.
Mitri HS, Edrissi R, Henning JG. 1995. Finite-element modeling of cable-bolted stopes in hard-rock underground mines. Trans Soc Min Metall Explor Inc. 298:1897–1902.
Nicholson GA, Bieniawski ZT. 1990. A nonlinear deformation modulus based on rock mass classification. Int J Min Geol Eng. 8(3):181–202.
Read SAL, Perrin ND, Richards LR. 1999. Applicability of the Hoek-Brown failure criterion to New Zealand greywacke rocks. In 9th ISRM Congress. Paris: international Society for Rock Mechanics and Rock Engineering.
Rocscience. 2022. RocData. Rocscience Inc.
Rocscience. 2022. RS2. Rocscience Inc.
Senent S, Mollon G, Jimenez R. 2013. Tunnel face stability in heavily fractured rock masses that follow the Hoek-Brown failure criterion. Int J Rock Mech Min Sci. 60:440–451.
Serafim JL. 1983. Consideration of the geomechanical classification of Bieniawski. In Proc int symp on engineering geology and underground construction. Vol. 1. Lisbon; p. 33–44.
Sonmez H, Gokceoglu C, Ulusay R. 2004. Indirect determination of the modulus of deformation of rock masses based on the GSI system. Int J Rock Mech Min Sci. 41(5):849–857.
Tang SB, Li JM, Ding S, Zhang LT. 2022. The influence of water-stress loading sequences on the creep behavior of granite. Bull Eng Geol Environ. 81(11):482.
Toraño J, Díez R, Rivas Cid JM, Barciella M. 2002. FEM modeling of roadways driven in a fractured rock mass under a longwall influence. Comput Geotech. 29(6):411–431.
Verman M, Singh B, Viladkar MN, Jethwa JL. 1997. Effect of tunnel depth on modulus of deformation of rock mass. Rock Mech Rock Engng. 30(3):121–127.
Wang GJ. 2005. Mechanical state of jointed rock mass and support structure of large tunnel during construction process. Chin J Rock Mech Eng. 24(8):1328–1334.
Wang Y, Zhu C, He MC, Wang X, Le HL. 2022. Macro-meso dynamic fracture behaviors of Xinjiang marble exposed to freeze thaw and frequent impact disturbance loads: a lab-scale testing. Geomech Geophys Geo-Energ Geo-Resour. 8(5):154.
Zhu C, Xu XD, Wang XT, Xiong F, Tao ZG, Lin Y, Chen J. 2019. Experimental investigation on nonlinear flow anisotropy behavior in fracture media. Geofluids 2019(9):1–9. article ID: 5874849.

Appendix A

Physical and mechanical parameters of intact rocks.

Location	Density (kg/m^3)	UCS (MPa)	Tensile strength (MPa)	Elastic modulus (GPa)	Poisson's ratio	Cohesion (MPa)	Internal friction angle (°)
−212 m	2718	39.18	5.3	33.85	0.235	8.48	40.4
−307 m	2722	45.52	4.9	38.75	0.23	15.63	41.4
−373 m	2748	78.15	5.9	44.90	0.22	10.62	50.8

Appendix B

Empirical equations for calculation of E_{mass}.

Equations (units GPa)	Equation No.	References	Remarks
$E_{mass} = 2RMR - 100$	(4)	(Bieniawski 1978)	For RMR > 50
$E_{mass} = 10^{(RMR-10)/40}$	(5)	(Serafim 1983)	For RMR < 50
$E_{mass} = 25\log_{10}Q$	(6)	(Barton et al. 1981)	For $Q > 1$
$E_{mass} = \frac{E_i}{100}(0.0028RMR^2 + 0.9\exp\left(\frac{RMR}{22.8}\right))$	(7)	(Nicholson and Bieniawski 1990)	
$E_{mass} = E_i(0.5(1-\cos(\pi RMR/100)))$	(8)	(Mitri et al. 1995)	
$E_{mass} = 0.3(H)^{\alpha}10^{(RMR-20)/38}$	(9)	(Verman et al. 1997)	
$E_{mass} = 0.1(RMR/10)^3$	(10)	(Read et al. 1999)	
$E_{mass} = 10(Q_c)^{1/3}$	(11)	(Barton 2002)	$Q_c = Q\frac{\sigma_{ci}}{100}$
$E_{mass} = (1 - D/2)\sqrt{\sigma_{ci}/100}\cdot 10^{(GSI-10)/40}$	(12)	(Marinos and Hoek 2000)	For $\sigma_{ci} \leq 100$
$E_{mass} = (1 - D/2)\cdot 10^{(GSI-10)/40}$			For $\sigma_{ci} > 100$
$E_{mass} = E_i(s^a)^{0.4}$	(13)	(Sonmez et al. 2004)	
$E_{mass} = E_i\left(0.02 + \frac{1-D/2}{1+e^{((60+15D-GSI)/11)}}\right)$	(14)	(Hoek and Diederichs 2006)	

Note: σ_{ci} is the uniaxial compression strength of intact rock, MPa. E_i is the elastic modulus of intact rock, GPa. $\alpha = 0.16 - 0.35$, 0.16 for hard rocks and 0.35 for weak rocks. H is the depth, m.